ADVANCING EARTH AND SPACE SCIENCES

JGR Atmospheres

RESEARCH ARTICLE
10.1029/2024JD041543

Key Points:

- Dust impacts on high clouds are highly nonlinear processes, while mechanisms depending on both meteorology and dust loadings
- Principal Component Analysis of meteorological factors reveals a dominant pattern that strongly controls global high cloud properties
- By isolating the dual effects of meteorology and ice water path, the specific impacts of dust on high cloud are clearly revealed

Supporting Information:

Supporting Information may be found in the online version of this article.

Correspondence to:
J. Ge,
gejm@lzu.edu.cn

Citation:
Mu, Q., Ge, J., Huang, J., Li, Q., Hu, X., Xia, Y., et al. (2025). Disentangling global dust-high cloud nonlinear interactions through multivariate meteorological constraints framework. *Journal of Geophysical Research: Atmospheres*, *130*, e2024JD041543. https://doi.org/10.1029/2024JD041543

Received 8 MAY 2024
Accepted 31 JAN 2025

Disentangling Global Dust-High Cloud Nonlinear Interactions Through Multivariate Meteorological Constraints Framework

Qingyu Mu[1], Jinming Ge[1], Jianping Huang[1], Qinghao Li[1], Xiaoyu Hu[2,3], Yang Xia[1], Zeen Zhu[4], Bo Wang[1], and Nan Peng[1]

[1]Key Laboratory for Semi-Arid Climate Change of the Ministry of Education and College of Atmospheric Sciences, Lanzhou University, Lanzhou, China, [2]Chongqing Research Institute of Big Data, Peking University, Chongqing, China, [3]School of Mathematical Sciences, Peking University, Beijing, China, [4]Environmental and Climate Sciences Department, Brookhaven National Laboratory, Upton, NY, USA

Abstract Dust aerosols, highly efficient ice nucleating particles, significantly influence high cloud properties, thereby impacting climate. As global warming and aridification are projected to increase dust emissions, understanding dust-high cloud interactions becomes increasingly crucial. However, disentangling dust effects from meteorology influences on high clouds remains challenging. This study employs Principal Component Analysis to derive the first principal component (PC1), a comprehensive indicator that characterizes meteorological conditions dominating high cloud evolution. This allows us to classify atmospheric conditions as weak (characterized by weak updrafts, low humidity, and stable atmosphere), moderate, or favorable (strong updrafts, high humidity, and unstable atmosphere). By strictly constraining both meteorological conditions and ice water path, we establish a framework to isolate dust impacts on high cloud. Our results unveil nonlinear dust-cloud interactions co-modulated by meteorology and dust loadings, contrary to previously assumed uniformity. Under weak meteorological conditions, dust impacts vary with loadings: low dust loadings promote larger ice crystals and denser clouds, while high dust levels lead to smaller crystals and thinner clouds. However, under favorable meteorological conditions, dust effects become notably weaker and remain relatively consistent across levels. These findings help explain previously conflicting observations of dust impacts on high clouds and highlight why both meteorological conditions and dust levels must be considered when studying dust-cloud interactions in a changing climate.

Plain Language Summary High clouds, composed primarily of ice crystals, play a crucial role in Earth's energy balance. These clouds form and evolve through interactions with dust particles, which serve as seeds for ice crystal formation. However, understanding how dust affects these clouds has been challenging since weather conditions also strongly influence cloud development. Using statistical method called principal component analysis, we identified dominant weather patterns affecting high clouds and isolate how these clouds really respond to different dust levels under varying weather conditions. Our findings reveal that dust's impact varies strongly with weather and its own levels. When weather conditions are unfavorable for cloud formation (with weak upward air motion and low moisture), dust has a significant but varying effect: small amounts of dust promote larger ice crystals and denser clouds, while large amounts lead to smaller crystals and thinner, more spread-out clouds. However, when weather conditions are favorable for cloud formation (with strong upward air motion and high moisture), dust has surprisingly little influence on cloud properties, regardless of its loadings. These results highlight how weather conditions play a crucial role in controlling dust-cloud interactions, potentially helping us better predict their combined effects on Earth's climate system.

1. Introduction

High clouds, formed at high altitudes and primarily composed of ice crystals, cover approximately 40% of the Earth's surface (Stubenrauch et al., 2013). They significantly modulate the global radiation budget by reflecting solar radiation and trapping longwave radiation (Fu & Liou, 1993; Lohmann & Gasparini, 2017), resulting in a net positive radiative effect that can considerably enhance the greenhouse effect (Matus & L'Ecuyer, 2017). High clouds also influence precipitation patterns and the global hydrologic cycle through the formation and growth of ice particles. These profound effects on the climate are intricately tied to and influenced by high cloud properties. Ice particles in high clouds conventionally originate via homogeneous freezing below 235 K under appropriate humidity (Pruppacher & Klett, 2010). However, certain aerosols can serve as ice nucleating particles (INPs), effectively reducing the meteorological barrier to ice crystal formation and initiating heterogeneous nucleation (Kärcher & Lohmann, 2003). This process can dominate high cloud formation and significantly influences their micro- and macro-physical properties (Cziczo et al., 2013; KÄrcher & Jensen, 2017). Therefore, understanding the impact of INP-capable aerosols on high cloud properties, known as aerosol-cloud interaction (ACI), is crucial for elucidating high clouds climate impacts.

Dust, widely dispersed across the globe, is recognized as a highly effective INP (Cziczo et al., 2004; Froyd et al., 2022). Originating from major deserts such as the Sahara and the Taklamakan, dust aerosols can ascend into the upper troposphere (Ge et al., 2016; Yang et al., 2022), forming a persistent dust layer along westerly belt in the Northern Hemisphere. Recent studies suggest that these dust aerosols are instrumental in 75%–93% of cirrus cloud formation in the Northern Hemisphere (Froyd et al., 2022). The substantial influence of dust on ice cloud radiative properties can directly reduce local incident solar radiation by up to 20 W m^{-2} during European dust events (Bangert et al., 2012). This interaction can also strengthen the large scale susceptibility of Indian summer monsoon precipitation (Patel et al., 2019). As anticipated increases in dust emission due to global warming (Bi et al., 2024; S. Chen, Wen, et al., 2023; Dayanandan et al., 2021), understanding the dust ACI effect becomes increasingly imperative for both weather and climate research. However, high cloud properties and their evolution are largely driven by meteorological conditions. Aircraft observations indicate that meteorological factors such as temperature, relative humidity, atmospheric stability, etc., have more significant impacts on ice crystal properties during the lifespan of cirrus clouds than the presence of aerosols (Patnaude & Diao, 2020). Parcel model simulations even suggest that strong vertical velocities can reduce the sensitivity of ice crystal response to INPs (Jensen et al., 2016). Consequently, differentiating meteorological impacts from dust aerosols on high clouds, as well as comprehending high cloud responses to varying dust loadings under diverse meteorological conditions are essential for advancing our grasp of dust ACI effects.

Prior research has typically focused on single meteorological factors when analyzing their effects on high clouds. For instance, Mitchell et al. (2018) and Kawamoto et al. (2020) employed temperature ranges as constraints, while Zhao and Gu et al. (2018) carried out discussion on ACI at different humidity levels. Other variables, such as vertical velocity and stability, also have been incorporated as restriction (Patnaude et al., 2021; Zhao, Liou, et al., 2018). However, high cloud formation and development depend on the complex interplay of multiple meteorological factors that often change together. While humidity strongly influences cloud development, it frequently varies alongside other conditions like atmospheric subsidence, which can inhibit cloud development (Chen, Wen, et al., 2023). This interconnected nature of meteorological factors suggests that studying them individually may not capture their combined effect on clouds.

Considering that cloud evolution is associated with dynamic changes in meteorological factors across a much broader range compared with clear sky conditions, the maximum co-variation direction among multiple key meteorological factors should align well with cloudy sky conditions. Thus, we propose utilizing the Principal Component Analysis (PCA) method to extract this dominant direction, also known as the first principal component (PC1), to indicate meteorological conditions for cloud evolution. PC1 can serve as a comprehensive indicator that combines the effects of temperature, humidity, vertical motion, and atmospheric stability into a single measure. It has also been validated to be highly correlated with cloud properties in our previous studies from long term ground-based cloud radar observations and reanalysis meteorology data at both the Semi-arid Climate and Environment Observatory of Lanzhou University (SACOL) and the Southern Great Plains atmospheric observatory (SGP) (Dong et al., 2023; Ge et al., 2019). These findings motivate us to expand the application of the PCA for isolating global-scale meteorology, enabling a deeper analysis of high cloud responses to dust aerosol.

In this study, we first identify key meteorological factors controlling high clouds and derive their PC1 pattern at global scale, as detailed in Section 2. Section 3.1 examines how high cloud properties vary with dust loadings and meteorological conditions by analyzing cloud behavior under PC1 constraints and different IWP. In Section 3.2, we combine PC1 and IWP into a comprehensive framework to isolate meteorological effects on high cloud properties, followed by detailed analysis of these varying dust effects. Section 3.3 introduces the ACI-index—defined as the negative logarithmic ratio of ice particle radius (IPR) to DAOD—to evaluate how different types of high clouds respond to dust. This analysis reveals complex dust-cloud interactions under varying conditions. Finally, Section 4 examines the underlying mechanisms driving these interactions.

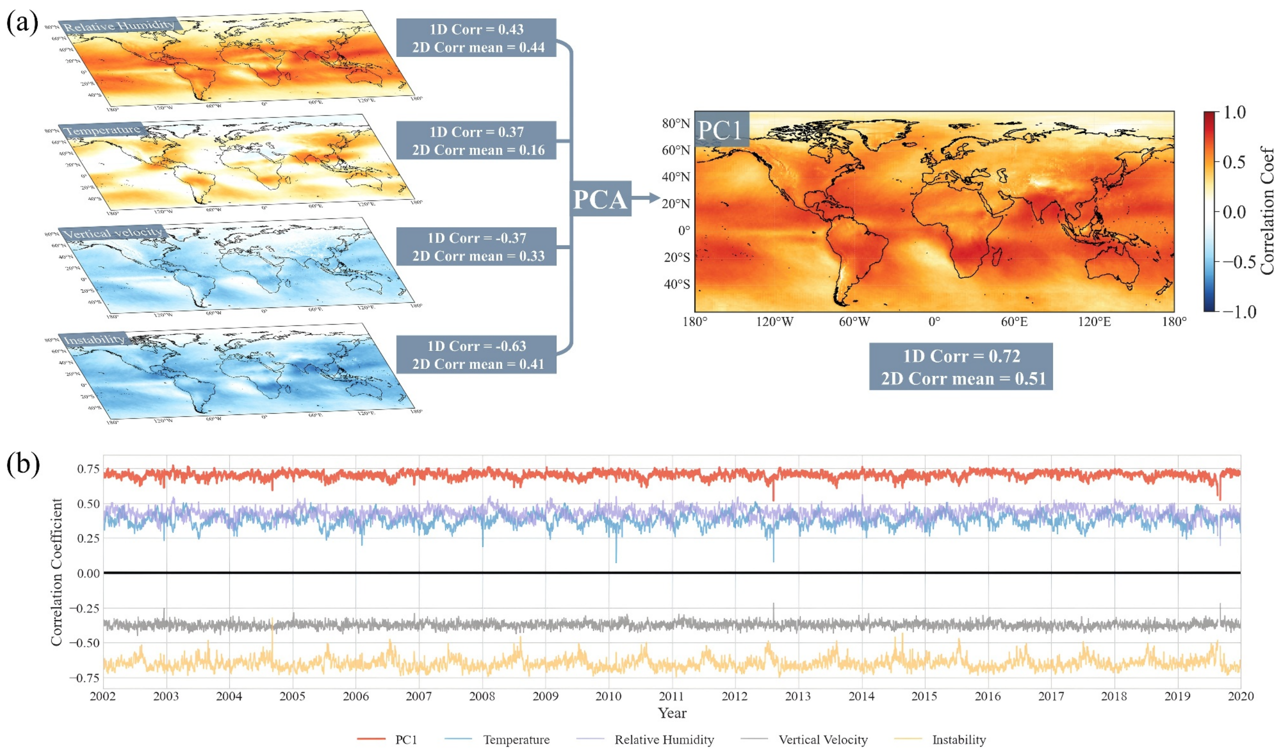

Figure 1. (a) Spatial distribution of correlation coefficients between RH_{250}, T_{250}, $Instab_{250-300}$, ω_{250}, PC1, and HCF, with each grid point exceed the critical value for significance at the 99% confidence level (1D Corr means that the data of these 19 years are uniformly transformed into a one-dimensional array and then the correlation coefficients are solved, and 2D Corr means that the correlation coefficients on each grid point are calculated and then averaged); (b) Correlation coefficients of each meteorological variable and PC1 on the 19-year time series with HCF respectively, with correlation coefficients calculated from the reshaped 1-dimensional array of daily spatial grids. Note that the Antarctic region was removed from this study because of the poor correlation between almost all meteorological factors, PC1 and HCF, details in Text S1 in Supporting Information S1.

2. Data and Methodology

2.1. Data Sets and Aerosol-Cloud Interaction Metrics

We adopt a 19-year (2002–2020) global meteorological fields from the European Center for Medium-Range Weather Forecasts Reanalysis v5 (ERA5, Hersbach et al., 2020) to establish a constraint for high cloud properties from satellite observations. ERA5 is generated using high-precision 4D-Var assimilation, providing validated high-resolution atmospheric factors (Sun & Fu, 2021). Four key factors at the 250 hPa pressure level were selected to extract PC1 (Dong et al., 2023; Ge et al., 2019): temperature (T_{250}), relative humidity (RH_{250}), vertical velocity (ω_{250}), and convective instability ($Instab_{250-300}$) derived from the equivalent potential temperature gradient between 250 hPa and 300 hPa. These variables were chosen not only for their statistical significance but also for their representation of fundamental atmospheric processes crucial for cloud development, as they capture thermal conditions, moisture availability, dynamical forcing, and overall atmosphere stability, respectively. These factors exhibited reasonable correlations with HCF, with correlation coefficients of 0.43, 0.37, −0.37, and −0.63, respectively (Figure 1).

High cloud properties during the same period were obtained from the Clouds and the Earth's Radiant Energy System Single Scanner Footprint (CERES SSF) data set, sourced from the Moderate Resolution Imaging Spectroradiometer (MODIS) aboard the Aqua satellite, with a spatial resolution of $1° \times 1°$ and daily averaged temporal resolution. We focus solely on high cloud properties in the 300-50 hPa layer, including high cloud area fraction (HCF), which refers to the fraction of the area covered by clouds in each region, cloud effective pressure (CEP), IWP, IPR, and cloud visible optical depth (COD). These macro- and micro-physical high cloud features help us examine how high clouds respond to dust aerosol.

DAOD, widely used as a proxy for dust loadings in ACI studies (Anoruo, 2020; Várnai et al., 2017), was sourced from the Modern-Era Retrospective analysis for Research and Applications, Version 2 (MERRA-2) gridded aerosol reanalysis data set (Gelaro et al., 2017). MERRA-2 assimilates multiple satellite and in situ observations, showing good alignment with direct measurements (Gueymard & Yang, 2020; Navinya et al., 2020). We interpolated the original MERRA-2 DAOD ($0.5° \times 0.625°$ resolution) to match our $1° \times 1°$ analysis grid (ERA5 & CERES SSF data). While MERRA-2's column-integrated DAOD introduces some uncertainty in vertical aerosol distribution, our comparison with CALIPSO upper-level measurements showed a good agreement (see Figures S2 and S3 and Text S2 in Supporting Information S1). MERRA-2 provides crucial advantages for this study: fine temporal resolution (3-hr means averaged to daily values), long-term coverage, and reliable measurements even under cloudy conditions through its Goddard Aerosol Assimilation System (Jia et al., 2021). These features make MERRA-2 a suitable data set for our analysis, despite some limitations in resolving vertical aerosol layers.

Leveraging these cloud property data and DAOD data, we applied the ACI-index, a widely used metric to quantify the strength of ACI. The ACI-index is generally defined as cloud susceptibility (Feingold et al., 2001):

$$\text{ACI index} = -\frac{d \ln \text{Cld}}{d \ln \text{Aer}} \tag{1}$$

where Cld represents cloud properties and Aer represents aerosol properties. In our study, we specifically examined how IPR responds to changes in DAOD, expressing the ACI-index as:

$$\text{ACI index} = -\frac{d \ln(\text{IPR})}{d \ln(\text{DAOD})} \tag{2}$$

This formulation, widely adopted in recent studies (Y. Yang et al., 2021; Zheng et al., 2020), allows us to quantify the nonlinear relationships between dust loading and high cloud properties, providing insights into how dust aerosols influence cloud microphysics.

2.2. PCA Method

To extract PC1 of T_{250}, RH_{250}, ω_{250}, and $\text{Instab}_{250-300}$, each factor was standardized to mitigate discrepancies arising from differing units. The standardized factors, originally in multidimensional arrays with temporal and spatial dimensions, were reshaped into a two-dimensional matrix. Each column of this matrix represented a meteorological factor, while the rows contain the temporal-spatial data points. The covariance matrix was then computed to obtain eigenvectors and eigenvalues, with the largest eigenvalue corresponding to PC1, which captured 41% of the total variance of all four meteorological factors. The one-dimensional PC1 was reshaped back into a multidimensional matrix to match the original temporal and spatial dimensions of the meteorological factors, serving as an integrated meteorological indicator for high cloud evolutions.

PC1's effectiveness was evaluated in controlling high cloud evolution through multiple correlation analyses (Figure 1). The one-dimensional correlation between PC1 and HCF—calculated from reshaped spatiotemporal distributions—reached 0.72, indicating a strong relationship. The two-dimensional global average correlation of 0.51, derived from grid-point time series correlations, confirms this relationship holds across both local and global scales. PC1 shows stronger correlations with cloud properties than any single meteorological factor, even in regions with few high clouds like subtropical subsidence zones and high latitudes. The consistency of PC1's relationship with HCF is demonstrated by stable daily correlation coefficients (0.68–0.74) throughout 2002–2020 (Figure 1b). These strong positive relationships highlight the robustness of PC1 as an integrated indicator of high cloud evolution across both space and time.

The physical interpretation of PC1 values is clarified by linking them with individual factors, as shown in Figure 2. Negative PC1 values indicate conditions unfavorable for high cloud development: sinking airflow (positive ω_{250}), low relative humidity ($\text{RH}_{250} < 60\%$), and near stable atmosphere, often associated with subsidence zones. These conditions are less conducive to high cloud formation through dynamical processes such as gravity waves, which require atmospheric instability to propagate and influence cloud formation. Whereas PC1 values near 1 represent moderate conditions with weak updrafts, higher humidity ($\text{RH}_{250} \sim 80\%$), and increasing instability. Notably, RH tends to saturate near PC1 = 1 (Figure 2a), limiting its effectiveness as an indicator of conditions conducive to further high cloud development beyond this point. Here, PC1 offers a distinct advantage over traditional methods that rely solely on RH_{250}. By integrating RH_{250}, ω_{250}, temperature, and instability, PC1

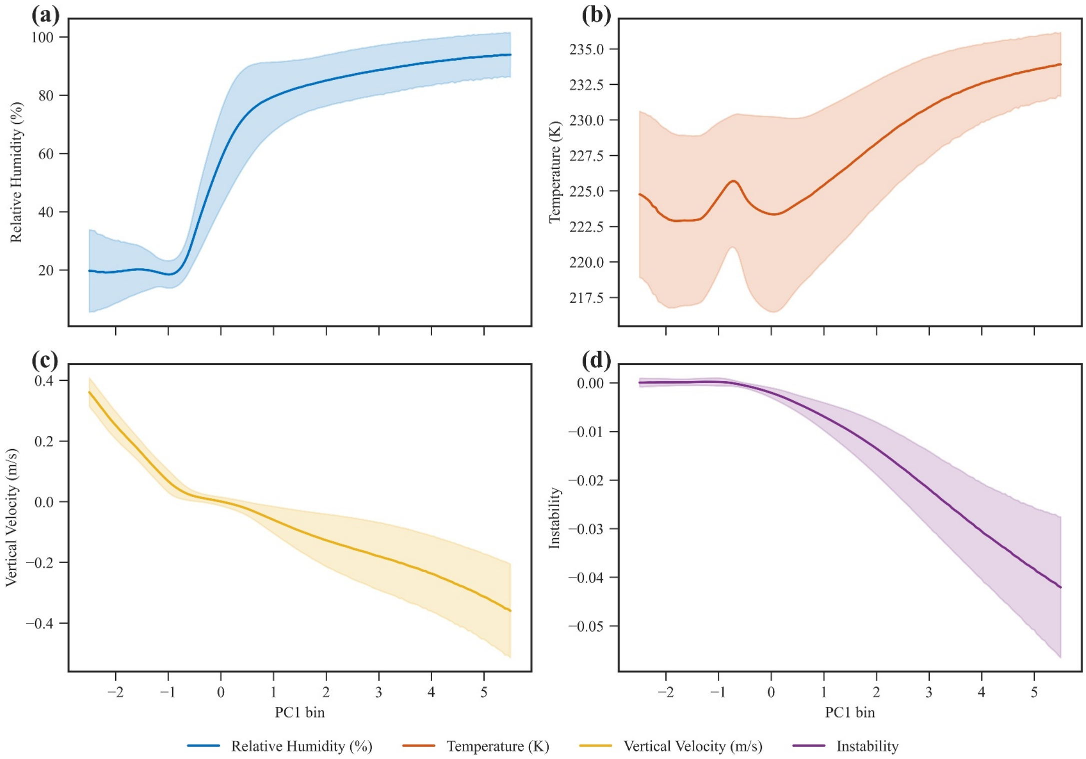

Figure 2. The variations in the four variables corresponding to the PC1 value, (a–d) denote relative humidity, temperature, vertical velocity, and convective instability, respectively, and the filled area denotes the standard deviation of the variable at this PC1 value.

provides a more comprehensive measure of meteorological conditions, particularly when RH is saturated. For instance, while RH plateaus, higher PC1 values still correspond to stronger updrafts and increased instability (Figures 2c and 2d), factors crucial for continued high cloud development. PC1 values above 3 denotes conditions highly favorable for cloud development, with strong updrafts and significant instability, typically found in regions of deep convection within the Intertropical Convergence Zone (ITCZ). Based on these distinct characteristics, we classify meteorological conditions as weak (PC1 < 0), moderate (0 < PC1 < 3), and favorable (PC1 > 3) for high cloud evolution. While PC1's relationship with individual meteorological factors is not strictly linear (Figure 2), it effectively captures their combined complex influence on cloud development. For instance, high humidity can occur with either strong subsidence or weak updrafts, depending on temperature and stability conditions. Through PCA projection, PC1 inherently incorporates these interactions, distilling the most relevant aspects of these variables for cloud development. This results in PC1's strong linear correlation with HCF, despite the underlying complex relationships among meteorological factors. This robust relationship between PCA and HCF establishes a solid foundation for our subsequent investigations of dust effects on high clouds under varying atmospheric conditions.

3. Results

3.1. PC1 and Ice Water Path Integrated Constraint Framework

The ACI effect is typically quantified through cloud susceptibility–the ratio of relative changes in cloud to relative variations in aerosol levels ($\frac{d \ln \mathrm{Cld}}{d \ln \mathrm{Aer}}$, logarithmic derivatives are used here to express the relative sensitivity of cloud to changes in aerosol, $\frac{d\,\mathrm{Cld}/\mathrm{Cld}}{d\,\mathrm{Aer}/\mathrm{Aer}} = \frac{d \ln \mathrm{Cld}}{d \ln \mathrm{Aer}}$). While the specific properties can vary (Feingold et al., 2022; Rosenfeld et al., 2019), the concept is to quantify the overall impact of aerosol on cloud changes. However, clouds respond not only to aerosols but also to meteorological conditions (hereby PC1) and available cloud water (IWP). These additional influences contribute significantly to uncertainty in ACI measurements but are often simply treated as “residual terms” in other studies (Gryspeerdt et al., 2014).

Cloud properties can be expressed as a multivariable function: $\mathrm{Cld} = f(\mathrm{Aer}, \mathrm{PC1}, \mathrm{IWP})$. Using the chain rule, the total derivative of cloud properties with respect to aerosols includes both ACI and indirect influences through meteorology and cloud water content:

$$\frac{d \ln \mathrm{Cld}}{d \ln \mathrm{Aer}} = \frac{\partial \ln \mathrm{Cld}}{\partial \ln \mathrm{Aer}} + \mathrm{Residuals} = \frac{\partial \ln \mathrm{Cld}}{\partial \ln \mathrm{Aer}} + \frac{\partial \ln \mathrm{Cld}}{\partial \ln \mathrm{PC1}} \frac{d \ln \mathrm{PC1}}{d \ln \mathrm{Aer}} + \frac{\partial \ln \mathrm{Cld}}{\partial \ln \mathrm{IWP}} \frac{d \ln \mathrm{IWP}}{d \ln \mathrm{Aer}} \tag{3}$$

Here, $\frac{\partial \ln \mathrm{Cld}}{\partial \ln \mathrm{Aer}}$ represents direct aerosols impact, while the remaining terms capture indirect influences through meteorological conditions and cloud water content. In actual atmosphere, these effects are intertwined, making it challenging to isolate the pure aerosol impact. Our framework addresses this challenge by simultaneously controlling both PC1 and IWP. When PC1 is held constant, variations in clouds, aerosols, and cloud water content become independent of meteorological conditions. Further accounting for IWP eliminates cloud variations due to cloud water content changes. Under these constraints, the relationship can be simplified to:

$$\frac{d \ln \mathrm{Cld}}{d \ln \mathrm{Aer}} = \frac{\partial \ln \mathrm{Cld}}{\partial \ln \mathrm{Aer}} \tag{4}$$

This final expression shows that under our dual constraints, the total derivative of cloud with respect to aerosols reduces to just the partial derivative, representing the solely dust-cloud interaction isolated from meteorological and cloud water influences. This dual-constraint approach provides a framework for our subsequent analysis of how dust directly affects high clouds, paving the way for our subsequent analysis.

Figure 3 presents the relationship between PC1 and high cloud properties under varying IWP and DAOD levels. PC1 effectively captures the influence of meteorological factors on cloud properties across a broad spectrum. Favorable meteorological conditions, indicated by high PC1 values, lead to an increase in HCF and a decrease in CEP, demonstrating that PC1 effectively isolates high cloud property variations in both horizontal extension and vertical development. Additionally, the cloud water effect remains significant in affecting cloud properties; under a given meteorological condition, larger IWP corresponds to higher HCF and IPR, suggesting that substantial cloud water supply is necessary for high cloud extension and ice crystal growth alongside meteorological influences (Figures 3a–3c).

Furthermore, the relationship between PC1 and cloud properties exhibits varying curve shapes depending on DAOD levels (Figures 3d–3f). Statistical significance tests (Mann-Whitney U tests, detailed in Text S3 in Supporting Information S1) confirmed that cloud properties significantly differ across DAOD levels within each PC1-IWP constraint, as indicated by asterisks in the figure. Under PC1 constraints, varying dust loadings do modulate cloud characteristics. However, the overall impact of DAOD is relatively modest compared to the dominant effects of PC1 and IWP. This is because the dust represents perturbations to cloud properties, which can be masked by the meteorological conditions encapsulated by PC1 and IWP. Consequently, in regions of the PC1 spectrum where meteorological influences are strong, the differences in cloud properties across DAOD levels become less pronounced, particularly in certain PC1 intervals affecting CEP. Nonetheless, the statistically significant differences affirm the crucial role of DAOD in modulating cloud characteristics, albeit as a secondary factor to meteorology and cloud water content. Hence, establishing the PC1-IWP constraint framework is crucial for distinguishing direct dust effects on high cloud properties from meteorological and other residual term effects. These dust ACI effects will be detailed in Section 3.2.

3.2. Nonlinear Dust Effects Unveiled Under Robust Constraints

Figure 4 shows how cloud properties vary within the PC1-IWP framework and how different dust levels impact ACI effect under various conditions. We divided the DAOD data into four groups with uneven bin sizes but equal sample data volumes, as DAOD data volumes decrease exponentially with increasing concentration. To ensure statistical robustness, we applied a 2000-data volume threshold for initial filtering and conducted Mann-Whitney U tests between adjacent DAOD levels at each PC1-IWP grid point. The Benjamini-Hochberg (BH) procedure was further used to correct for multiple comparisons under 95% levels. Only statistically significant differences are shown in Figures 3e–3h, with detailed statistical methods provided in the Text S3 in Supporting Information S1.

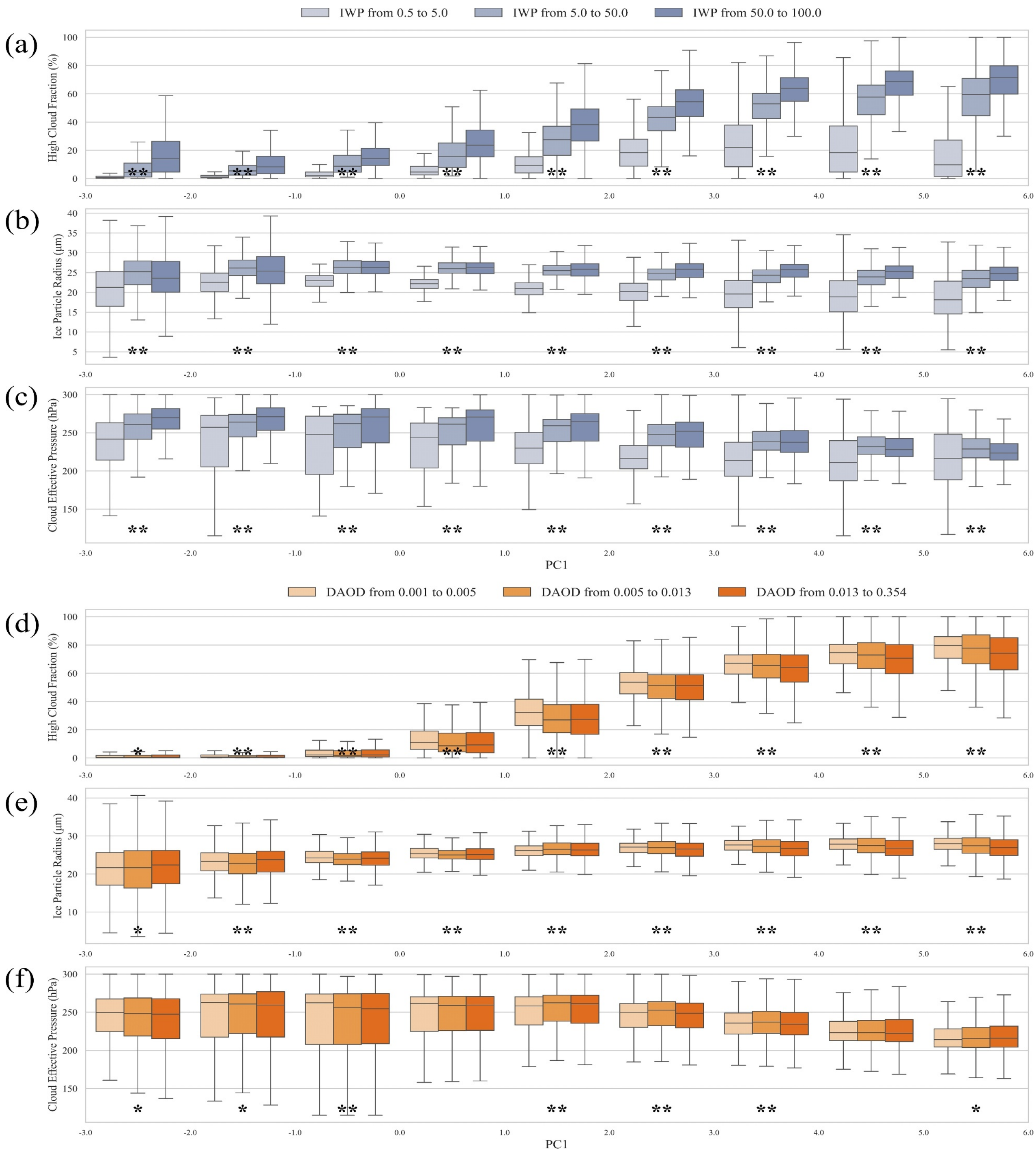

Figure 3. Relationships between meteorological conditions (PC1) and high cloud macroscopic and microphysical properties, varying with different ice water path (IWP) and DAOD levels. In Figures 2a–2f, darker blue and red colors indicate higher IWP and DAOD, respectively. Asterisks (*) denote statistically significant differences in a PC1 bin between 2 IWP or DAOD groups ($p < 0.05$), and double asterisks (**) indicate significance across all IWP or DAOD groups ($p < 0.01$) (Detail of significant test can be referred by Text S3 in Supporting Information S1).

At the macroscopic level, the framework captures the promotional effect of meteorology on cloud macroscopic development, with high HCF areas concentrated in the upper-right quadrant across the four slices (Figure 4a). The PC1 effectively distinguishes between high and low values of CEP, which also steadily rise with increased IWP (Figure 4b). At the microscopic level, meteorological influences on high clouds manifest subtle controls rather

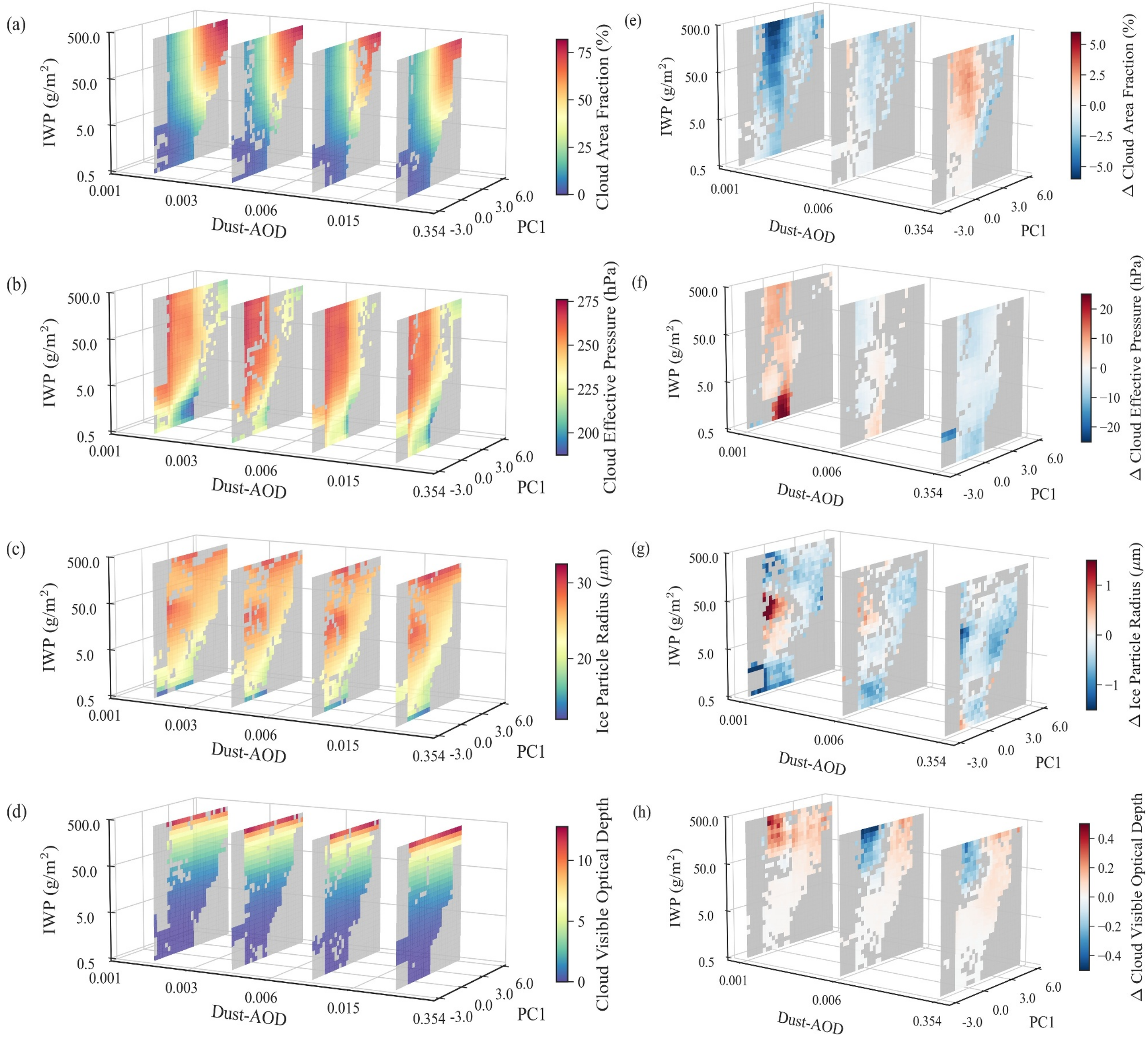

Figure 4. Macro- and microphysical quantities of high clouds under the multi-constraints of PC1, DAOD, and ice water path. HCF (a, e), CEP (b, f), ice particle radius (c, g), and COD (d, h) are shown in each row from top to bottom. The first column (a–d) denotes the high cloud properties, while the second column (e–h) illustrates the variations of these properties with increasing DAOD. Blue color indicates a decrease, and red color indicates an increase with rising DAOD. The first column (a–d) only shows statistically significant variations ($p < 0.05$) with increasing DAOD after applying BH correction and grid points with more than 2000 data volume. The second column (e–h) only calculate grid points in the first column which passed significant test. Detailed data volumes are provided in Figure S4 in Supporting Information S1, significance test details are provided in Supporting Information S1.

than simply promoting or suppressing cloud growth. Two distinct IPR peaks across various dust levels are revealed under this framework (Figure 4c). The first peak is associated with thin clouds under relatively weak meteorology and low cloud-water scenarios, while the second peak appears under favorable meteorology with sufficient cloud water supply. COD exhibits a near-linear relationship with IWP, indicating its high dependence on cloud vertical development (Figure 4d). It can also be observed that PC1 exhibits a weak but discernible influence on COD variations especially under high IWP conditions, complementary to the primary IWP effect.

To isolate dust's influence on cloud properties within this framework, we further analyze how cloud characteristics change between adjacent DAOD intervals at each PC1-IWP grid point. Specifically, we calculate the difference in cloud properties between successive DAOD levels using:

$$\Delta \mathrm{Cld}(i,j)_{\mathrm{DAOD\ level}\ z} = \mathrm{Cld}(i,j)_{\mathrm{DAOD\ level}\ z+1} - \mathrm{Cld}(i,j)_{\mathrm{DAOD\ level}\ z} \tag{5}$$

where i,j represent i *th* PC1 bin and j *th* IWP bin, respectively. $\mathrm{Cld}(i,j)_{\mathrm{DAOD\ level}\ z+1}$ and $\mathrm{Cld}(i,j)_{\mathrm{DAOD\ level}\ z}$ represents cloud properties at specific PC1-IWP grid point under DAOD level $z + 1$ and z. The term $\Delta \mathrm{Cld}(i,j)_{\mathrm{DAOD\ level}\ z}$ can herein reveal how cloud properties respond to increasing dust concentrations while maintaining consistent meteorological and cloud water conditions, allowing us to disentangle dust's impacts on cloud development.

Figures 4e–4h show the isolated changes in cloud properties attributed to variations in dust loadings. For weak meteorology (PC1 < 0) with relatively moderate cloud-water ($10\ \mathrm{g\ m^{-2}} < \mathrm{IWP} < 50\ \mathrm{g\ m^{-2}}$), high clouds typically exhibit small HCF, thin optical depth and low cloud height, indicating an unsuitable environment for ice crystal formation. However, when PC1-IWP is held constant (i.e., within the same region in each slice), the IPR tendency exhibits a more prominent variation with increasing DAOD compared with other conditions, suggesting that dust aerosols exert the most prominent influence on the size of ice particles under these conditions. We also note that the effect of dust on ice crystals, and thus high clouds, varies with its loadings under such conditions.

At minimal dust levels (DAOD ≈ 0.001), dust increases IPR and COD under moderate cloud-water ($10\ \mathrm{g\ m^{-2}} < \mathrm{IWP} < 50\ \mathrm{g\ m^{-2}}$), supporting high clouds' higher sensitivity to dust nucleation effect. The enlarged ice particles restrict the spatial development of clouds, resulting in denser high clouds with large ice crystals. As the DAOD increases to 0.006, the IPR growth trend weakens (Figure 4g), while cloud coverage and height begin to increase (Figures 4e and 4f), accompanied by a decline in COD (Figure 4h). This shift in the dust impact on clouds becomes more evident at high DAOD levels (DAOD ≈ 0.354), where dust tends to reduce ice particle size and enhance the horizontal and vertical cloud development. The observed transition from increasing IPR to decreasing IPR as dust loadings increase suggests that the impact mechanism of dust on high clouds varies under different meteorological conditions. We propose that dust-induced evaporation, caused by its light-absorbing nature (Ge et al., 2010; Tang et al., 2016), may become more prominent than its nucleation effect at high dust levels, leading to a reduction in IPR. Moreover, an abundance of dust nuclei can lead to intensified competition for water vapor among ice crystals under such weak meteorological conditions, further decreasing IPR and potentially reducing the overall concentration of ice crystals. Consequently, the high clouds formed tend to have smaller and fewer ice crystals under these conditions, creating "lighter" clouds that exhibit greater horizontal and vertical development than those formed under low dust scenarios.

As meteorological conditions enhance from weak to moderate (0 < PC1 < 2), the sensitivity of nearly all cloud physical properties to dust gradually diminishes, as evidenced by the fading red and blue colors in Figures 4e–4h. When meteorological conditions further intensify to strong (PC1 > 3), high clouds exhibit markedly reduced sensitivity to dust, displaying a minimal and almost consistent response across a wide range of dust levels. This is characterized by a slight decrease in cloud coverage (Figure 4e) and ice crystal size (Figure 4g) with dust impact. The intense updraft and high humidity characteristic of the meteorological field can rapidly lift dust-induced ice crystals to the upper atmosphere, limiting their growth (Sullivan et al., 2017). This process, coupled with an unstable atmosphere, increases the probability of ice particle collision and fragmentation (Grzegorczyk et al., 2023; Phillips, 2021), leading to the formation of smaller ice particles. In contrast to weak and moderate meteorology, which may not support the nucleation of excessive dust, favorable meteorological conditions are sufficient for dust-induced ice nucleation. Thus, while IPR is reduced, the concentration of ice particles due to dust likely increases under these conditions, resulting in an overall increase in COD. On the macroscopic scale, these ice particles result in decreased HCF. The intense meteorological conditions are likely causing this cloud coverage reduction through rapid mixing and evaporation at the cloud edges or the formation of precipitation, as also pointed out by previous studies (Christensen et al., 2020).

Our constraint framework reveals the nonlinear effects of dust on high clouds, with PC1 serving as an integrated meteorological indicator that clearly outlines the different dust impact mechanisms under varying conditions. Under relatively weak meteorology and low dust loadings, dust enhances ice particle growth. While at higher concentrations, dust exhibits inhibitory effects, reducing ice particle size and resulting in thinner clouds. As meteorological conditions intensify, the sensitivity of high clouds to dust diminishes, with dust effects remaining relatively constant across concentrations. These findings pave the way for our further exploration of the varying dust effects observed in different types of high clouds and their spatial distributions.

10.1029/2024JD041543

3.3. Distinctive Dust Impacts Across Various Cloud Types

High clouds form through diverse mechanisms and exhibit varying degrees of vertical development, which significantly influence their interactions with dust (Zhao, Gu, et al., 2018). To better understand the spatial distribution of ACI effects among these different types of high cloud, we classify them into four groups using IWP as a measure of vertical development: low (<1 g m^{-2}), mid-low (1–10 g m^{-2}), mid-high (10–100 g m^{-2}), and high IWP (>100 g m^{-2}). This classification enables the identification of regions where specific types of high clouds exhibit distinct responses to dust and allows us to investigate how these effects vary with meteorology. To ensure consistency, DAOD levels are categorized as: low (0.001–0.003), medium (0.003–0.015), and high (0.015–0.354). Using these classifications, we calculate the ACI-index, where negative values indicate dust increases ice crystal size, while positive values show it decreases size.

Our results reveal that while dust impacts high clouds differently across IWP levels, these interactions consistently exhibit strong dependence on both dust loading and meteorological conditions. For low IWP clouds, which predominantly appear in subtropical high-pressure zones with relatively low PC1 values (Figures 5a and 5b, and S6a in Supporting Information S1), we observe complex dust-cloud interactions. In these regions, dust initially reduces ice crystal size at all DAOD levels, consistent with observations of anvil clouds (Fan et al., 2013), indicating dust's inhibition of thin ice cloud development under weak meteorological conditions. However, as meteorology becomes more favorable, dust's impact shifts from inhibiting to promoting ice crystal growth. This pattern holds true even in our region-specific analysis of the subsidence zone (30°S–5°N, 105°W–175°W), characterized by extremely weak updrafts and low humidity (Figure S7 in Supporting Information S1, top panel). The consistency between the global (Figure 5b) and regional (Figure S7 in Supporting Information S1) analyses suggests that this effect is not merely an artifact of large-scale averaging but reflects a genuine physical mechanism. Intriguingly, the turning point for the shift of ACI-index from positive to negative depends on dust loading and meteorological conditions. High dust loadings can trigger ice crystal formation under relatively weak meteorological conditions (PC1 $\approx$ 0.4), transitioning from shrinking to enlarging ice crystals due to abundant dust nuclei. In contrast, lower dust loadings require stronger meteorological conditions to achieve the same effect. While moderate dust concentrations show a similar transition at PC1 $\approx$ 1.5, limited data points make this interpretation more tentative.

For mid-low IWP levels, high clouds transition from high-pressure zones to complex terrain areas, which are regions with relatively high altitudes and significant altitude fluctuations (Figure S6b in Supporting Information S1). Despite differing cloud formation mechanisms, their ACI-index curves show similar trends (Figures 5d and 5f), dividing into dust sensitive and insensitive segments depending on meteorology. Under weak to moderate meteorological conditions (PC1 < 2), dust exhibits nonlinear effects on clouds: increasing IPR at low to moderate dust levels and decreasing them at high level. The enhancement effect is more pronounced at low DAOD levels compared to moderate DAOD levels, suggesting that under conditions of limited cloud water, low dust loadings can avoid excessive competition for water vapor, fostering more significant ice crystal growth. However, as meteorological conditions strengthen (PC1 > 2), the dust-induced effects on IPR become nearly indistinguishable across dust levels. This results in ACI-index values that are almost identical, reflecting that the ACI effects under these stronger meteorological conditions are nearly the same regardless of dust loading. The additional region-specific analysis focusing only the complex terrain zone (10°N–50°N, 30°E−100°E), encompassing areas such as the Iranian Plateau and Arabian Plateau, confirmed these dust effects are consistent both in the global analysis and within specific complex terrain regions (Figure S7 in Supporting Information S1, middle panel). The pattern also continues into mid-high IWP level high clouds (Figures 5e and 5f), where clouds are concentrated in the ITCZ regions.

As for high IWP levels, where high clouds are tightly associated with deep convection (Figures 5g and 5h, and S6d in Supporting Information S1), dust effects differ from other types of high clouds. The convective atmosphere and sufficient water vapor facilitate ice particle formation. At low dust loadings, due to low dust nuclei, homogeneous nucleation likely dominates, forming numerous small ice particles. As dust loadings increase to moderate and high levels, heterogeneous nucleation may become more prevalent. The increased abundance of dust nuclei can scavenge water vapor and suppress homogeneous nucleation (He et al., 2022), leading to the formation of larger ice crystals. Consequently, the effect of dust in reducing ice particle size is less pronounced at moderate to high dust levels (Figure 5h). This mechanism also explains the blurred phenomenon observed in high IWP regions of Figure 4g, where dust reduces IPR at low DAOD levels but show mini-impact at higher levels,

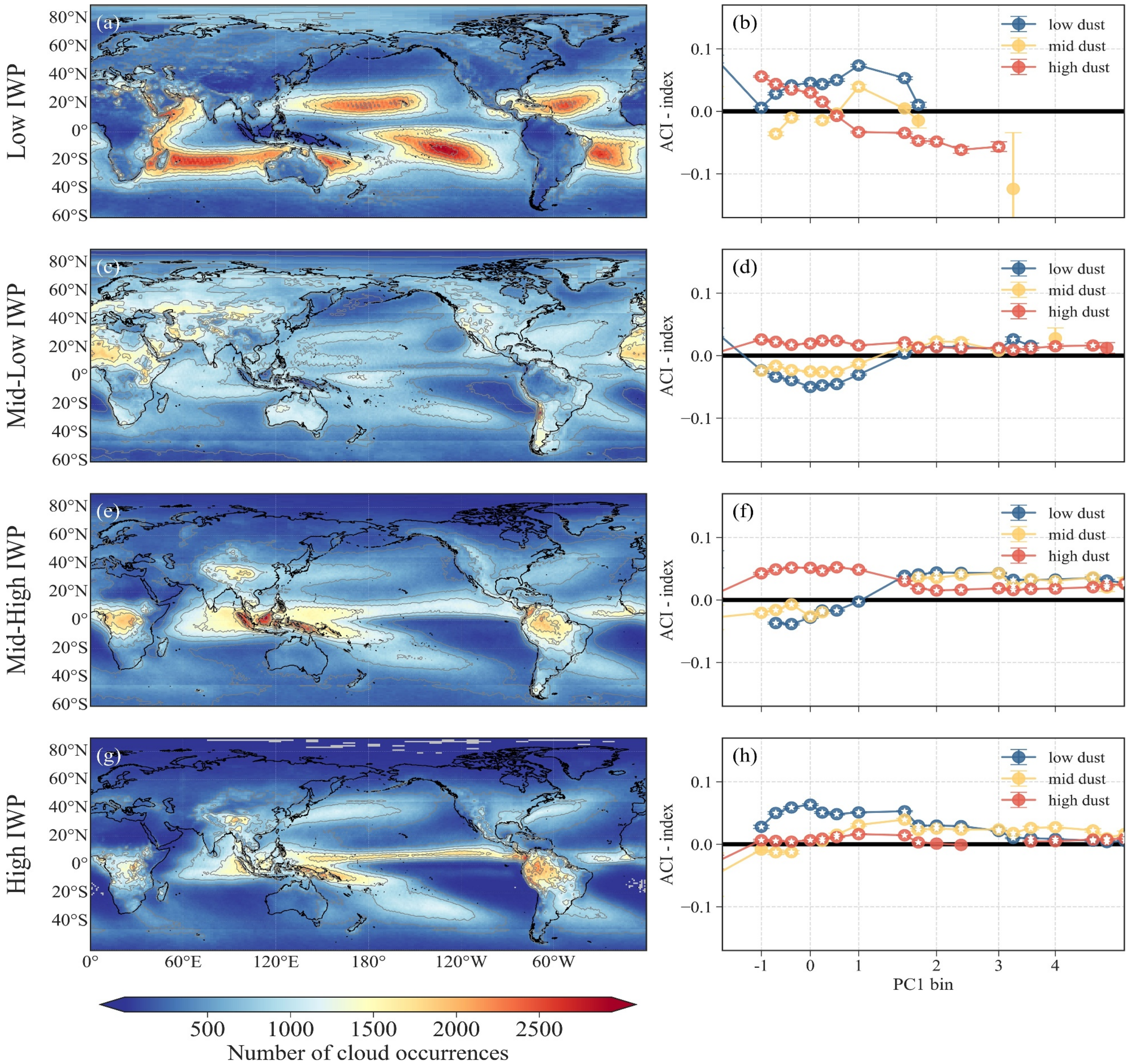

Figure 5. Spatial distribution of high cloud types according to ice water path (IWP) and their corresponding ACI-index curves. Panels (a, c, e, and g) show the number of occurrences of high clouds in each IWP interval. Panels (b, d, f, and h) present the ACI-index values for high clouds in each IWP interval, with blue, yellow, and red colors representing low, medium, and high dust loadings, respectively. White asterisks denote statistically significant ACI-index values ($p < 0.05$), while points were excluded if the error value exceeded the absolute value of the ACI-index. The error bar represents double standard deviation.

complementing the understanding of the nonlinear dust-effect in various types of high clouds. Nonetheless, when meteorology becomes highly favorable (PC1 > 3), the effect of dust on these clouds diminishes rapidly, with the ACI-index approaching zero. The consistency between this global analysis and the region-specific deep convection zone (20°S−20°N, 70°E−170°E) analysis (Figure S7 in Supporting Information S1, bottom panel) reinforces the robustness of our statements, demonstrating that these patterns are not unique to specific regions but represent a general feature of dust-high cloud interactions under strong meteorological forcing.

4. Schematic of the Intricate Dust Effects on High Clouds

By extracting the integrated meteorological indicator of PC1 at global scale, the proposed PC1-IWP constraint framework effectively untangles the dust impacts from the meteorological effects on high cloud properties. Our

10.1029/2024JD041543

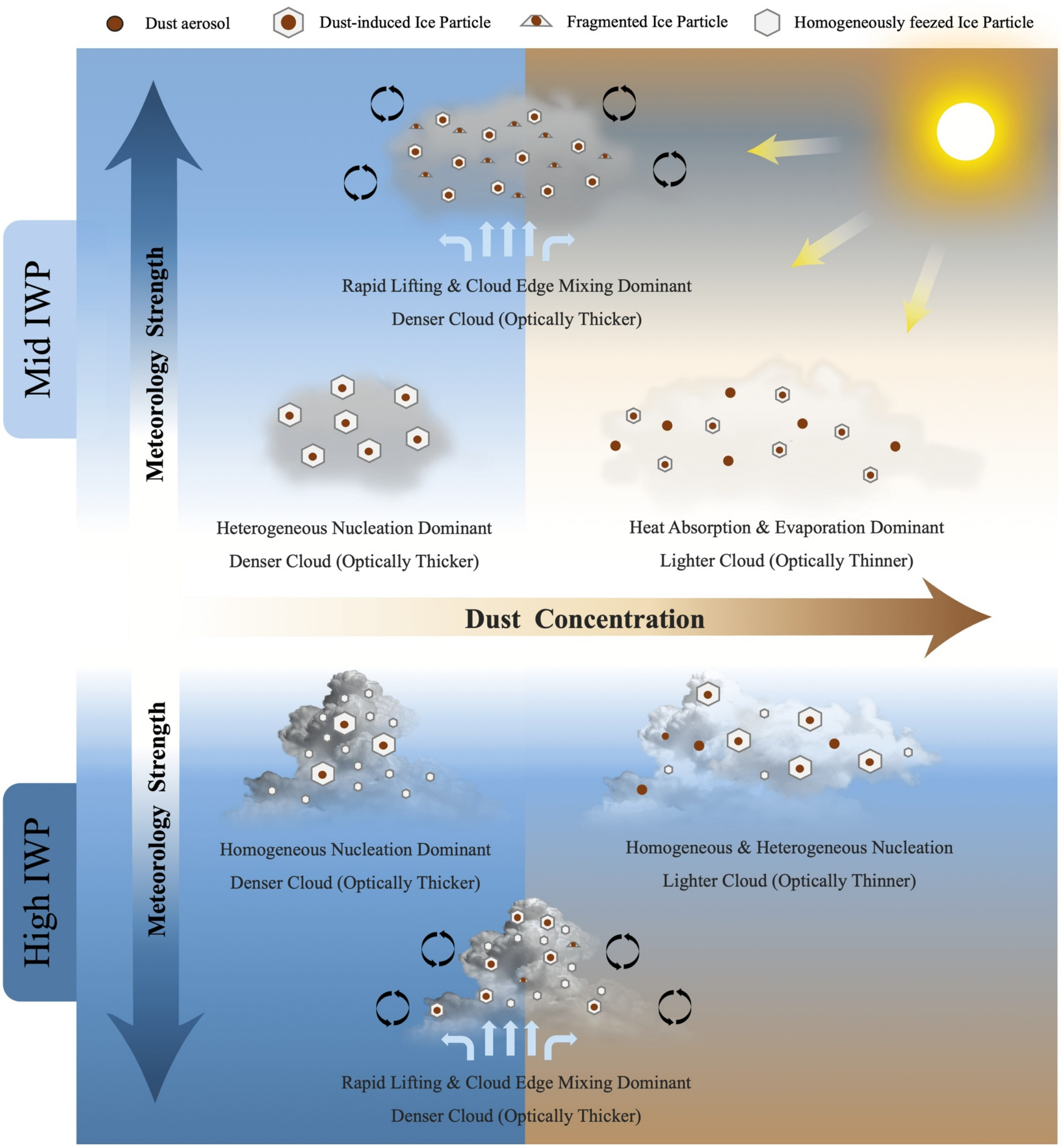

Figure 6. Schematic representation of nonlinear dust effects on high clouds, co-modulated by meteorology and dust loading. Darker blue represents high ice water path (IWP), deeper brown indicates higher dust levels, and darker clouds show greater optical thickness. For mid IWP under weak meteorology, low dust levels lead to larger ice crystals and denser clouds, while high dust levels reduce ice growth, causing cloud expansion and thinning due to dust evaporation. For high IWP under weak meteorology, low dust levels result in smaller ice crystals and denser clouds via homogeneous nucleation, while high dust levels reduce ice shrinkage due to a trade-off between nucleation types. Under strong meteorology, dust causes smaller ice crystals, greater optical thickness, and reduced cloud coverage, regardless of dust loading. Dust impacts weaken with strong updrafts and edge mixing (clouds in these conditions are shown in the middle of the dust loading axis).

study unveils the nonlinear dust effects on high clouds, which are co-modulated by meteorology, cloud water supply, and dust loading, as illustrated in Figure 6.

Under weak meteorology (PC1 < 0), dust impacts on high clouds are most pronounced. At low dust loadings, dust particles act as efficient INPs, promoting heterogeneous nucleation. This leads to the formation of larger ice crystals and denser, optically thicker clouds (depicted as larger ice crystals and darker clouds in the schematic). The enhanced ice crystal growth under these conditions is due to the availability of dust particles facilitating ice nucleation in an environment otherwise unfavorable for cloud development. However, as dust loading rises to high levels under the same weak meteorology, the effect of dust shifts. Excessive dust can lead to competition for available water vapor, inhibiting ice crystal growth and resulting in smaller ice crystals. Additionally, dust's light-absorbing properties can induce the heat-absorbing evaporation effect, promoting evaporation of ice crystals. High clouds hence become thinner and more expansive horizontally (represented by smaller ice crystals and lighter, wider clouds in the schematic). In high IWP conditions, typically associated with convective clouds with abundant cloud water supply, the dust impact on high clouds exhibit additional nuances under weak meteorology. When cloud water content is abundant but meteorological conditions are weak, homogeneous nucleation can become dominant, leading to the formation of numerous small ice crystals in dense clouds. As dust loadings increase, heterogeneous nucleation becomes more prominent due to the abundance of INPs, resulting in relatively larger ice crystals compared to the low-dust scenario. At very high dust loadings, sufficient dust particles can in turn suppress homogeneous nucleation to certain extent, displaying relatively unchanged ice crystal size as also shown in Figures 4g and 5h. The complex interplay illustrates how dust loading, and cloud water availability can modulate ice crystal properties even under weak meteorological conditions.

As meteorological conditions strengthen ($0 < PC1 < 2$), the sensitivity of high clouds to dust begins to diminish. Under strong meteorology ($PC1 > 3$), characterized by strong updrafts, high humidity, and unstable atmosphere, the impact of dust on high clouds becomes nearly independent of dust loading (illustrated by similar-sized ice crystals and cloud properties across different dust loadings in the schematic). Fast updrafts rapidly lift ice crystals, limiting their growth time, and strong mixing reduces the influence of dust-induced nucleation processes. In both mid and high IWP scenarios, dust consistently leads to smaller ice crystals, but the overall effect is weak. Processes such as collisional fragmentation, driven by strong updrafts, and enhanced entrainment mixing at cloud edges contribute to this weakened dust effect.

By capturing this varying sensitivity of high clouds to dust under different meteorological conditions and dust loadings, our framework provides a comprehensive explanation for the diverse dust effects on various types of high clouds with different mechanisms across the globe. This unifying framework reconciles the seemingly disparate ACI phenomena reported in previous studies by providing a unified framework that accounts for the co-modulation by meteorology, cloud water content, and dust loadings. Furthermore, integrating nonlinear dust effects and their meteorological dependencies into climate models is essential for accurately predicting future climate scenarios, especially in the context of increasing dust emissions due to global warming and aridification.

5. Conclusions and Discussions

In this study, we developed an analytical framework to effectively isolate the combined influences of meteorology, cloud water content, and dust concentrations on high clouds. This framework decouples dust effects from meteorological influences on high cloud properties and their susceptibilities, revealing that dust can either promote or inhibit ice cloud development depending on atmospheric conditions. These findings offer insights into previously contradictory observations, such as the difficulties in simulating cirrus cloud cover during intense dust events (Nickovic et al., 2016; Weger et al., 2018), and the struggles in reconciling the contradictory phenomena, as observed by Santos et al. (2013), where opposing effects of dust on cloud optical thickness are observed at the same location.

While our framework reveals important patterns in dust-cloud interactions, we must acknowledge certain limitations. Our reanalysis data sets, though providing comprehensive global coverage, cannot fully capture fine-scale meteorological processes or aerosol variations, particularly in regions with complex terrain (Shestakova et al., 2024; Wang et al., 2023).

In addition, the use of column-integrated DAOD, while advantageous in mitigating cloud contamination biases, can introduce uncertainty regarding the precise altitude of dust layers. This is a common challenge in ACI studies, as highlighted by previous research (Tang et al., 2024). Although our large-scale statistical analysis helps offset some limitations through data volume (detailed discussion provided in Text S3 in Supporting Information S1), and MERRA-2 offers advantages over traditional satellite aerosol products in cloudy conditions, the results should be viewed as primarily qualitative rather than precise quantitative assessments. Precisely quantifying these effects—especially the transitions between different nucleation processes—still remains challenging. Therefore, our findings best serve as indicators of general patterns and mechanisms rather than exact numerical measurements.

Nevertheless, our results have important implications for climate modeling. The framework reveals why using a single ice nucleation parameterization scheme may lead to under- or overestimation of dust effects on cirrus clouds, explaining nearly twofold discrepancies in previous modeling studies (Kuebbeler et al., 2014; Lohmann et al., 2008). Our findings become particularly relevant as global warming increases precipitation over desert regions, as evidenced by recent intense rainfall events in the Taklimakan Desert during June 2023, Libya during September 2023, and the historic rainfall in the United Arab Emirates during April 2024. The complex interactions we identified between dust and ice clouds may help explain these unusual precipitation patterns in arid regions. As climate warming increases atmospheric water vapor content and instability (Santer et al., 2007), the combination of stronger meteorological conditions and abundant dust nuclei could enhance ice cloud development and trigger convective precipitation. We hypothesize that these nonlinear dust effects may further amplify precipitation variability alongside the increased precipitation variability already shown to occur (Zhang et al., 2021) in a warmer future.

Our study presents a unified framework to constrain the influence of meteorology on high cloud evolution and isolate the nonlinear effects of dust on high cloud properties. While uncertainties remain, the findings offer a new pathway to improve dust-cloud interaction simulations. We recommend implementing dynamic parameterization schemes that account for both meteorological conditions and aerosol concentrations. By incorporating the co-modulation of dust effects by meteorology and dust loadings, models can better capture these nonlinear interactions, ultimately improving our ability to predict future changes in radiation and precipitation patterns as dust-cloud interactions evolve with climate change.

Data Availability Statement

The ERA5 hourly data used in this study are held on the Climate Data Store (CDS) by the ECMWF (Hersbach et al., 2020). The CERES SSF1deg-Day data, sourced from the Aqua satellite Edition 4, is available on CERES official website (NASA/LARC/SD/ASDC, 2017). The MERRA-2 tavg1_2d_aer_Nx 2d_aer_Nx aerosol data set is accessible through Goddard Earth Sciences Data and Information Services Center (GES DISC) (Global Modeling And Assimilation Office & Pawson, 2015). Additionally, our analysis code are hosted publicly on Zenodo at (MacCanthy, 2024), enabling replication and further exploration of our findings.

Acknowledgments
This research is supported by the National Natural Science Foundation of China (Grant 41875028, 91937302, and 42275076), the Science and Technology Program of Gansu Province (Grant 22JR5RA398 and 24JRRA490), and the Fundamental Research Funds for the Central Universities (Grant lzujbky-2022-ct06). The author would like to thank Prof. Daniel Rosenfeld and Dr. Olivier Boucher for their comments on earlier versions of this study. All data and codes used in this study have been given in the Open Research section. More in-depth processed data can be obtained by contacting the author or corresponding author.

References

Anoruo, C. M. (2020). Space and ground-based remote sensing comparison of seasonal interaction of aerosol-cloud-precipitable water. *Atmospheric Environment*, *243*, 117864. https://doi.org/10.1016/j.atmosenv.2020.117864

Bangert, M., Nenes, A., Vogel, B., Vogel, H., Barahona, D., Karydis, V. A., et al. (2012). Saharan dust event impacts on cloud formation and radiation over Western Europe. *Atmospheric Chemistry and Physics*, *12*(9), 4045–4063. https://doi.org/10.5194/acp-12-4045-2012

Bi, H., Chen, S., Zhang, D., Wang, Y., Kang, L., Alam, K., et al. (2024). The circumglobal transport of massive African dust and its impacts on the regional circulation in remote atmosphere. *Bulletin of the American Meteorological Society*, *105*(3), E605–E622. https://doi.org/10.1175/BAMS-D-23-0072.1

Chen, R., Wen, Z., Lin, W., & Qiao, Y. (2023). Diverse relationship between the tropical night in south China and the water vapor transport over the South China Sea and the plausible causes. *Atmospheric Research*, *296*, 107080. https://doi.org/10.1016/j.atmosres.2023.107080

Chen, S., Chen, J., Zhang, Y., Lin, J., Bi, H., Song, H., et al. (2023). Anthropogenic dust: Sources, characteristics and emissions. *Environmental Research Letters*, *18*(10), 103002. https://doi.org/10.1088/1748-9326/acf479

Christensen, M. W., Jones, W. K., & Stier, P. (2020). Aerosols enhance cloud lifetime and brightness along the stratus-to-cumulus transition. *Proceedings of the National Academy of Sciences*, *117*(30), 17591–17598. https://doi.org/10.1073/pnas.1921231117

Cziczo, D. J., Froyd, K. D., Hoose, C., Jensen, E. J., Diao, M., Zondlo, M. A., et al. (2013). Clarifying the dominant sources and mechanisms of cirrus cloud formation. *Science*, *340*(6138), 1320–1324. https://doi.org/10.1126/science.1234145

Cziczo, D. J., Murphy, D. M., Hudson, P. K., & Thomson, D. S. (2004). Single particle measurements of the chemical composition of cirrus ice residue during CRYSTAL-FACE. *Journal of Geophysical Research*, *109*(D4), 2003JD004032. https://doi.org/10.1029/2003JD004032

Dayanandan, B., Patel, P. N., Tiwari, P., Al-Amri, I., Thakadiyil, S., Al-Badi, H., & Al-Riyami, K. (2021). Long-term changes in aerosol loading and observed impacts on radiative budget over the middle-east. *Environmental Sciences Proceedings*, *8*(1), 8. https://doi.org/10.3390/ecas2021-10695

Dong, Z., Ge, J., Gao, A., Zhu, Z., Yan, J., Mu, Q., et al. (2023). Comparisons of cirrus clouds and their linkages to meteorology at the SACOL and the SGP sites. *Atmospheric Research*, *281*, 106467. https://doi.org/10.1016/j.atmosres.2022.106467

Fan, J., Leung, L. R., Rosenfeld, D., Chen, Q., Li, Z., Zhang, J., & Yan, H. (2013). Microphysical effects determine macrophysical response for aerosol impacts on deep convective clouds. *Proceedings of the National Academy of Sciences*, *110*(48), E4581–E4590. https://doi.org/10.1073/pnas.1316830110

Feingold, G., Goren, T., & Yamaguchi, T. (2022). Quantifying albedo susceptibility biases in shallow clouds. *Atmospheric Chemistry and Physics*, *22*(5), 3303–3319. https://doi.org/10.5194/acp-22-3303-2022

Feingold, G., Remer, L. A., Ramaprasad, J., & Kaufman, Y. J. (2001). Analysis of smoke impact on clouds in Brazilian biomass burning regions: An extension of Twomey's approach. *Journal of Geophysical Research*, *106*(D19), 22907–22922. https://doi.org/10.1029/2001JD000732

Froyd, K. D., Yu, P., Schill, G. P., Brock, C. A., Kupc, A., Williamson, C. J., et al. (2022). Dominant role of mineral dust in cirrus cloud formation revealed by global-scale measurements. *Nature Geoscience*, *15*(3), 177–183. https://doi.org/10.1038/s41561-022-00901-w

Fu, Q., & Liou, K. N. (1993). Parameterization of the radiative properties of cirrus clouds. *Journal of the Atmospheric Sciences*, *50*(13), 2008–2025. https://doi.org/10.1175/1520-0469(1993)050<2008:POTRPO>2.0.CO;2

Ge, J., Wang, Z., Liu, Y., Su, J., Wang, C., & Dong, Z. (2019). Linkages between mid-latitude cirrus cloud properties and large-scale meteorology at the SACOL site. *Climate Dynamics*, *53*(7–8), 5035–5046. https://doi.org/10.1007/s00382-019-04843-9

Ge, J. M., Liu, H., Huang, J., & Fu, Q. (2016). Taklimakan desert nocturnal low-level jet: Climatology and dust activity. *Atmospheric Chemistry and Physics*, *16*(12), 7773–7783. https://doi.org/10.5194/acp-16-7773-2016

Ge, J. M., Su, J., Ackerman, T. P., Fu, Q., Huang, J. P., & Shi, J. S. (2010). Dust aerosol optical properties retrieval and radiative forcing over northwestern China during the 2008 China-US joint field experiment. *Journal of Geophysical Research*, *115*(D7), 2009JD013263. https://doi.org/10.1029/2009JD013263

Gelaro, R., McCarty, W., Suárez, M. J., Todling, R., Molod, A., Takacs, L., et al. (2017). The modern-era retrospective analysis for research and applications, version 2 (MERRA-2). *Journal of Climate*, *30*(14), 5419–5454. https://doi.org/10.1175/JCLI-D-16-0758.1

Global Modeling And Assimilation Office, & Pawson, S. (2015). MERRA-2 tavg1_2d_lnd_Nx: 2d,1-Hourly,Time-Averaged,Single-Level, Assimilation,Land surface diagnostics V5.12.4 [Dataset]. *NASA Goddard Earth Sciences Data and Information Services Center*. https://doi.org/10.5067/RKPHT8KC1Y1T

Gryspeerdt, E., Stier, P., & Grandey, B. S. (2014). Cloud fraction mediates the aerosol optical depth-cloud top height relationship. *Geophysical Research Letters*, *41*(10), 3622–3627. https://doi.org/10.1002/2014GL059524

Grzegorczyk, P., Yadav, S., Zanger, F., Theis, A., Mitra, S. K., Borrmann, S., & Szakáll, M. (2023). Fragmentation of ice particles: Laboratory experiments on graupel–graupel and graupel–snowflake collisions. *Atmospheric Chemistry and Physics*, *23*(20), 13505–13521. https://doi.org/10.5194/acp-23-13505-2023

Gueymard, C. A., & Yang, D. (2020). Worldwide validation of CAMS and MERRA-2 reanalysis aerosol optical depth products using 15 years of AERONET observations. *Atmospheric Environment*, *225*, 117216. https://doi.org/10.1016/j.atmosenv.2019.117216

He, Y., Yin, Z., Liu, F., & Yi, F. (2022). Technical note: Identification of two ice-nucleating regimes for dust-related cirrus clouds based on the relationship between number concentrations of ice-nucleating particles and ice crystals. *Atmospheric Chemistry and Physics*, *22*(19), 13067–13085. https://doi.org/10.5194/acp-22-13067-2022

Hersbach, H., Bell, B., Berrisford, P., Hirahara, S., Horányi, A., Muñoz-Sabater, J., et al. (2020). The ERA5 global reanalysis. *Quarterly Journal of the Royal Meteorological Society*, *146*(730), 1999–2049. https://doi.org/10.1002/qj.3803

Jensen, E. J., Ueyama, R., Pfister, L., Bui, T. V., Alexander, M. J., Podglajen, A., et al. (2016). High-frequency gravity waves and homogeneous ice nucleation in tropical tropopause layer cirrus. *Geophysical Research Letters*, *43*(12), 6629–6635. https://doi.org/10.1002/2016GL069426

Jia, H., Ma, X., Yu, F., & Quaas, J. (2021). Significant underestimation of radiative forcing by aerosol–cloud interactions derived from satellite-based methods. *Nature Communications*, *12*(1), 3649. https://doi.org/10.1038/s41467-021-23888-1

KÄrcher, B., & Jensen, E. J. (2017). Microscale characteristics of homogeneous freezing events in cirrus clouds. *Geophysical Research Letters*, *44*(4), 2027–2034. https://doi.org/10.1002/2016GL072486

Kärcher, B., & Lohmann, U. (2003). A parameterization of cirrus cloud formation: Heterogeneous freezing. *Journal of Geophysical Research*, *108*(D14). https://doi.org/10.1029/2002JD003220

Kawamoto, K., Yamauchi, A., Suzuki, K., Okamoto, H., & Li, J. (2020). Effect of dust load on the cloud top ice-water partitioning over northern middle to high latitudes with CALIPSO products. *Geophysical Research Letters*, *47*(15), e2020GL088030. https://doi.org/10.1029/2020GL088030

Kuebbeler, M., Lohmann, U., Hendricks, J., & Kärcher, B. (2014). Dust ice nuclei effects on cirrus clouds. *Atmospheric Chemistry and Physics*, *14*(6), 3027–3046. https://doi.org/10.5194/acp-14-2014-3027

Lohmann, U., & Gasparini, B. (2017). A cirrus cloud climate dial? *Science*, *357*(6348), 248–249. https://doi.org/10.1126/science.aan3325

Lohmann, U., Spichtinger, P., Jess, S., Peter, T., & Smit, H. (2008). Cirrus cloud formation and ice supersaturated regions in a global climate model. *Environmental Research Letters*, *3*(4), 045022. https://doi.org/10.1088/1748-9326/3/4/045022

MacCanthy. (2024). muqingyu666/Project_Dust_ACI: DustACIunderPC1Constraint (DustACI) [Software]. *Zenodo*. https://doi.org/10.5281/zenodo.11057950

Matus, A. V., & L'Ecuyer, T. S. (2017). The role of cloud phase in Earth's radiation budget. *Journal of Geophysical Research: Atmospheres*, *122*(5), 2559–2578. https://doi.org/10.1002/2016JD025951

Mitchell, D. L., Garnier, A., Pelon, J., & Erfani, E. (2018). CALIPSO (IIR–CALIOP) retrievals of cirrus cloud ice-particle concentrations. *Atmospheric Chemistry and Physics*, *18*(23), 17325–17354. https://doi.org/10.5194/acp-18-17325-2018

NASA/LARC/SD/ASDC. (2017). CERES and GEO-enhanced TOA, within-atmosphere and surface fluxes, clouds and aerosols 1-hourly Terra-Aqua Edition4A. *NASA Langley Atmospheric Science Data Center DAAC*. https://doi.org/10.5067/TERRA+AQUA/CERES/SYN1DEG-1HOUR_L3.004A

Navinya, C. D., Vinoj, V., & Pandey, S. K. (2020). Evaluation of PM2.5 surface concentrations simulated by NASA's MERRA version 2 aerosol reanalysis over India and its relation to the air quality index. *Aerosol and Air Quality Research*, *20*(6), 1329–1339. https://doi.org/10.4209/aaqr.2019.12.0615

Nickovic, S., Cvetkovic, B., Madonna, F., Rosoldi, M., Pejanovic, G., Petkovic, S., & Nikolic, J. (2016). Cloud ice caused by atmospheric mineral dust – Part 1: Parameterization office nuclei concentration in the NMME-DREAM model. *Atmospheric Chemistry and Physics*, *16*(17), 11367–11378. https://doi.org/10.5194/acp-16-11367-2016

Patel, P. N., Gautam, R., Michibata, T., & Gadhavi, H. (2019). Strengthened Indian summer monsoon precipitation susceptibility linked to dust-induced ice cloud modification. *Geophysical Research Letters*, *46*(14), 8431–8441. https://doi.org/10.1029/2018GL081634

Patnaude, R., & Diao, M. (2020). Aerosol indirect effects on cirrus clouds based on global aircraft observations. *Geophysical Research Letters*, *47*(10), e2019GL086550. https://doi.org/10.1029/2019GL086550

Patnaude, R., Diao, M., Liu, X., & Chu, S. (2021). Effects of thermodynamics, dynamics and aerosols on cirrus clouds based on in situ observations and NCAR CAM6. *Atmospheric Chemistry and Physics*, *21*(3), 1835–1859. https://doi.org/10.5194/acp-21-1835-2021

Phillips, V. T. J. (2021). Ice multiplication by fragmentation during quasi-spherical freezing of raindrops: A theoretical investigation. *Journal of the Atmospheric Sciences*, *78*(10), 3215–3228. https://doi.org/10.1175/JAS-D-20-0309.1

Pruppacher, H. R., & Klett, J. D. (2010). Homogeneous nucleation. In H. R. Pruppacher & J. D. Klett (Eds.), *Microphysics of clouds and precipitation* (pp. 191–215). Springer Netherlands. https://doi.org/10.1007/978-0-306-48100-0_7

Rosenfeld, D., Zhu, Y., Wang, M., Zheng, Y., Goren, T., & Yu, S. (2019). Aerosol-driven droplet concentrations dominate coverage and water of oceanic low-level clouds. *Science*, *363*(6427), eaav0566. https://doi.org/10.1126/science.aav0566

Santer, B. D., Mears, C., Wentz, F. J., Taylor, K. E., Gleckler, P. J., Wigley, T. M. L., et al. (2007). Identification of human-induced changes in atmospheric moisture content. *Proceedings of the National Academy of Sciences*, *104*(39), 15248–15253. https://doi.org/10.1073/pnas.0702872104

Santos, D., Costa, M. J., Silva, A. M., & Salgado, R. (2013). Modeling saharan desert dust radiative effects on clouds. *Atmospheric Research*, *127*, 178–194. https://doi.org/10.1016/j.atmosres.2012.09.024

Shestakova, A. A., Fedotova, E. V., & Lyulyukin, V. S. (2024). Relevance of Era5 reanalysis for wind energy applications: Comparison with sodar observations. *Geography, Environment, Sustainability*, *17*(1), 54–66. https://doi.org/10.24057/2071-9388-2023-2782

Stubenrauch, C. J., Rossow, W. B., Kinne, S., Ackerman, S., Cesana, G., Chepfer, H., et al. (2013). Assessment of global cloud datasets from satellites: Project and database initiated by the GEWEX radiation panel. *Bulletin of the American Meteorological Society*, *94*(7), 1031–1049. https://doi.org/10.1175/BAMS-D-12-00117.1

Sullivan, S. C., Hoose, C., & Nenes, A. (2017). Investigating the contribution of secondary ice production to in-cloud ice crystal numbers. *Journal of Geophysical Research: Atmospheres*, *122*(17), 9391–9412. https://doi.org/10.1002/2017JD026546

Sun, L., & Fu, Y. (2021). A new merged dataset for analyzing clouds, precipitation and atmospheric parameters based on ERA5 reanalysis data and the measurements of the tropical rainfall measuring mission (TRMM) precipitation radar and visible and infrared scanner. *Earth System Science Data*, *13*(5), 2293–2306. https://doi.org/10.5194/essd-13-2293-2021

Tang, M., Cziczo, D. J., & Grassian, V. H. (2016). Interactions of water with mineral dust aerosol: Water adsorption, hygroscopicity, cloud condensation, and ice nucleation. *Chemical Reviews*, *116*(7), 4205–4259. https://doi.org/10.1021/acs.chemrev.5b00529

Tang, S., Wang, H., Li, X.-Y., Chen, J., Sorooshian, A., Zeng, X., et al. (2024). Understanding aerosol–cloud interactions using a single-column model for a cold-air outbreak case during the ACTIVATE campaign. *Atmospheric Chemistry and Physics*, *24*(17), 10073–10092. https://doi.org/10.5194/acp-24-10073-2024

Várnai, T., Marshak, A., & Eck, T. F. (2017). Observation-based study on aerosol optical depth and particle size in partly cloudy regions. *Journal of Geophysical Research: Atmospheres*, *122*(18), 10013–10024. https://doi.org/10.1002/2017JD027028

Wang, N., Tian, J., Su, S., & Tian, Q. (2023). A downscaling method based on MODIS product for hourly ERA5 reanalysis of land surface temperature. *Remote Sensing*, *15*(18), 4441. https://doi.org/10.3390/rs15184441

Weger, M., Heinold, B., Engler, C., Schumann, U., Seifert, A., Fößig, R., et al. (2018). The impact of mineral dust on cloud formation during the saharan dust event in April 2014 over europe. *Atmospheric Chemistry and Physics*, *18*(23), 17545–17572. https://doi.org/10.5194/acp-18-17545-2018

Yang, K., Wang, Z., Luo, T., Liu, X., & Wu, M. (2022). Upper troposphere dust belt formation processes vary seasonally and spatially in the northern hemisphere. *Communications Earth & Environment*, *3*(1), 24. https://doi.org/10.1038/s43247-022-00353-5

Yang, Y., Zhao, C., Wang, Y., Zhao, X., Sun, W., Yang, J., et al. (2021). Multi-source data based investigation of aerosol-cloud interaction over the North China Plain and North of the Yangtze Plain. *Journal of Geophysical Research: Atmospheres*, *126*(19), e2021JD035609. https://doi.org/10.1029/2021JD035609

Zhang, W., Furtado, K., Wu, P., Zhou, T., Chadwick, R., Marzin, C., et al. (2021). Increasing precipitation variability on daily-to-multiyear time scales in a warmer world. *Science Advances*, *7*(31), eabf8021. https://doi.org/10.1126/sciadv.abf8021

Zhao, B., Gu, Y., Liou, K., Wang, Y., Liu, X., Huang, L., et al. (2018). Type-dependent responses of ice cloud properties to aerosols from satellite retrievals. *Geophysical Research Letters*, *45*(7), 3297–3306. https://doi.org/10.1002/2018GL077261

Zhao, B., Liou, K.-N., Gu, Y., Jiang, J. H., Li, Q., Fu, R., et al. (2018). Impact of aerosols on ice crystal size. *Atmospheric Chemistry and Physics*, *18*(2), 1065–1078. https://doi.org/10.5194/acp-18-1065-2018

Zheng, X., Xi, B., Dong, X., Logan, T., Wang, Y., & Wu, P. (2020). Investigation of aerosol–cloud interactions under different absorptive aerosol regimes using Atmospheric Radiation Measurement (ARM) southern Great Plains (SGP) ground-based measurements. *Atmospheric Chemistry and Physics*, *20*(6), 3483–3501. https://doi.org/10.5194/acp-20-3483-2020